Computational Materials Science 146 (2018) 278–286

Contents lists available at ScienceDirect

Computational Materials Science

journal homepage: www.elsevier.com/locate/commatsci

A tight-binding molecular dynamics study of the noble metals Cu, Ag and Au

S. Silayi [a], D.A. Papaconstantopoulos [a,*], M.J. Mehl [b]

[a] Center for Simulation and Modeling & Department of Computational and Data Sciences, George Mason University, Fairfax, VA 22030, USA
[b] U.S. Naval Academy, Annapolis, MD 21402, USA

ARTICLE INFO

Article history:
Received 14 August 2017
Received in revised form 22 January 2018
Accepted 23 January 2018

Keywords:
Molecular dynamics
Tight-binding
Noble metals
Electronic structure

ABSTRACT

We have used the Naval Research Lab (NRL) tight-binding (TB) method to study the electronic and mechanical properties of the noble metals. In order to perform molecular dynamics simulations, we used new TB parameters that work well at smaller interatomic distances. The TB parameters were fitted to the fcc, bcc and sc periodic structures and were demonstrated to be transferable and robust for calculating additional dynamical properties which they had not been fitted to. We calculated the phonon frequencies and density of states at finite temperature and we also performed simulations to determine the temperature dependence of the coefficient of thermal expansion and the mean squared displacement. The energy for vacancy formation as well as energy for fcc-based, bcc-based clusters and icosahedral clusters of different sizes were also calculated. The results compared very well with experimental observations and independent (non-fitted) first-principles density functional calculations.

1. Introduction

The tight-binding method (TB) as first proposed by Slater and Koster [1] proved very accurate in the reproduction of first-principles data for the electronic band structures and density of states. To reproduce the electronic band structure of a system as well as the total energy and to ensure the transferability of TB parameters between different structures, the NRL-TB method was proposed [2,3] and was shown to predict results for the elastic moduli, equilibrium lattice constants, surface energies and phonon spectra for different materials that were in good agreement with experimental results. The method was also shown to reproduce first-principles total energies for several crystal structures that are not fitted [3].

Extending the NRL-TB method to molecular dynamics(MD) simulations, the model was shown to provide results for both static and dynamic properties of a number of materials that were in agreement with experimental observations over a range of temperatures [4,5]. This is significant because the static calculations had been limited to working out properties at the fixed temperature of $T = 0$ K while most actual processes occur at finite temperature. It is very important to stress here that part of the objective of this work is to extend the range of validity of the TB parameters used in Refs. [2,3] which, although work well for quantities calculated in those papers, fail in MD simulations.

The parameters initially calculated and used in the NRL-TB method have been very successful, resulting in accurate calculated structural properties as compared to the experimental [2,6]. In this work we develop new parameters which improve on those of Ref. [2] and apply them, producing results over a wider range of interatomic distances as would be encountered in a realistic MD simulation. The extended parameters were tested by calculating band structures, equilibrium lattice constants, total energy at different volumes for the fcc, bcc, simple cubic (sc), hexagonal closed packed (hcp) and diamond structures and the elastic constants. The calculated values were compared to both results calculated from parameters that had only been fit to interatomic distances close to equilibrium lattice constant.

There have been MD simulations that similarly explored different properties of the noble metals. For example, Kabir et al. [7] employed a minimal parameter TBMD scheme initially proposed by Menon et al. [8] to study the stable structures of Cu clusters. Zhao et al. [9] also used the same approach to study Ag clusters. A study on the bulk properties of the noble metals was done by Januszko and Bose [10]. Using the embedding function of Sutton and Chen [11] and a modified version of the same by Kimura et al. [12], they were able to calculate the phonon spectra and a number of thermodynamic properties for the noble metals such as the thermal expansion coefficient, bulk modulus and specific

* Corresponding author.
E-mail address: dpapacon@gmu.edu (D.A. Papaconstantopoulos).

https://doi.org/10.1016/j.commatsci.2018.01.046
0927-0256/

heat constants and compared results from using the different approaches. While such empirical potential methods are much faster than the first principles methods, they do have a cost as far as accuracy and transferability is concerned because they do not include quantum mechanics (QM). The TB method falls in between the two approaches, so that although it is only in the range of three orders of magnitude faster than the first principles calculations, it is more accurate and covers a much wider range of applications than the empirical methods.

For our study, we performed a series of MD simulations at various temperatures to determine the temperature dependence of the electronic DOS, mean square displacement and the related Debye-Waller factors for Cu, Ag and Au. Additionally, we calculated the thermal expansion coefficients, energies of vacancy formation, cluster energies and phonon frequencies for a range of temperatures and compared the results to experimental observations.

The results from fcc, bcc and icosahedron cluster energy calculations were compared to asses how the energies and configurations for relaxed clusters behaved relative to each other. Cluster energies were also calculated using DFT first principles methods for comparison with the results from the new parametrizations.

2. Simulation details

2.1. The NRL-TB method

This method is a Slater-Koster-like method which is similar to the Huckel approach used in Chemistry. It has been applied to most single elements as well as to binary and a few ternary systems. The method performs very well in metals, insulators and semiconductors and in this paper we explore the transferability of our TB parameters to clusters. The method is based on fitting parameters to density functional theory (DFT) results. It works in both an orthogonal and non-orthogonal basis and computes both the individual energy levels (bands in the case of periodic solids) and the total energy of the system. It has atom-density dependent onsite parameters and distance dependent hopping and overlap parameters in the form of polynomials given by the equations in the appendix. The resulting Hamiltonian has transferability far beyond the fitted DFT database, and therefore is capable of performing MD simulations that accommodate as many as 10,000 atoms and 10,000 MD steps, which is an impractical task for standard DFT codes. The NRL-TB was originally built for an *spd* Hamiltonian (corresponding to a secular equation of size 9×9 per atom) and recently extended [14] to include f-electron states resulting in 16×16 secular equations.

The NRL-TB method retains the QM basis of DFT, is almost exact regarding the fitted DFT structures and provides reasonable predictions for structures that are not fitted. In summary, the NRL-TB method can be viewed as a bridge from DFT to empirical potential approaches, being about 1000 times faster than DFT and retaining the QM character of DFT. On the contrary, empirical potential approaches are much faster than TB but because they do not include QM principles, their transferability to non-fitted (to experiment or DFT) quantities is limited.

2.2. The fitting process

In the fitting process to calculate the new TB parameters and extend their validity to smaller inter-atomic distances we used the linearized augmented plane wave (LAPW) method [15–17] to generate a data insert of the band structures and total energies as a function of the volume for fcc, bcc and sc structures. The TB parameters are obtained by fitting to the LAPW results reproduce band structures and total energies as a function of volume for the fcc, bcc and sc crystal structures very accurately. Earlier TB parameters as used in Refs. [2,3] work well for quantities calculated in those papers but fail in MD simulations. The reason is that in the orthogonal TB representation we are using, the overlap matrix has negative eigenvalues (non-positive definite) for smaller lattice constants than those used in the fit. As a result, the total energy turns down at the smaller inter-atomic distances in which the MD would take the simulation (as shown in Fig. 1)

The extended range of the lattice constants at which the resulting TB Hamiltonian becomes suitable for MD simulations, $a \approx 0.88a_0$, is shown in Table 1. It was critical to include lower lattice constant data to produce parameters that would work in a wide range of interatomic distances as occurs in MD simulations. We also show in Table 1 the corresponding pressure values for the lowest lattice parameter used in the fit. The rms error of the fit is 0.1 mRy for the total energy and 3 mRy for the six bands fitted.

These new parameters were then tested by recalculating total energy as a function of volume for the different structures. In the plotted results in Fig. 2 we show the total energy versus volume for the three structures and the hcp structure which was not fitted, and is close to the fcc as expected. We also calculated the total energy for the diamond lattice which was found to be high in energy, as expected [2], and is not shown in Fig. 2. Calculations to show the transferability of the new TB parameters gave results (shown in Table 1) that accurately matched both experimental data and earlier calculations done using different parameters [2,5].

Using the new parameters, MD simulations were done to calculate the DOS at finite temperature, the Debye-Waller factor as derived from the Mean Square Displacement calculations, the thermal expansion coefficient and the phonon frequencies. Additional simulations were done for the single and double vacancy formation energies. To further demonstrate the high quality and robustness of our TB Hamiltonians we calculated total energies of fcc and bcc clusters energies for all the three noble metals.

Kirchhoff et al. [14] had calculated some dynamical properties for Au using the extended parameters such as the DOS and phonons at finite temperature. Here, we present more extensive calculations to check the robustness of the parameters together with the extended parameters of the other two noble metals, Cu and Ag.

2.3. TBMD simulation (microcanonical run)

The simulation is initialized with a supercell of 125 atoms arranged in the fcc crystal structure which is the equilibrium structure for the noble metals. The initialized primitive cell is translated

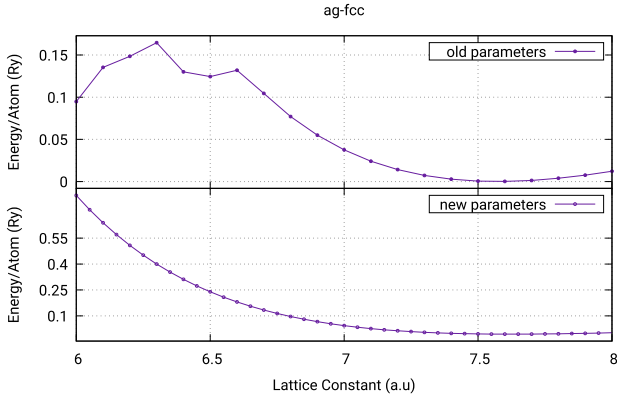

Fig. 1. The new parameters have improved behavior at smaller lattice constant values when compared to previously calculated parameters. The plot demonstrates behavior of the old and new parameters for Ag.

Table 1
Calculated bulk modulus and elastic constants in Mbar for Ag, Au and Cu. Measured values are taken from Simmons and Wang, Ref. [13]. Values for pressure (P_a) in GPa at the lowest fitted lattice constant (a) in a.u. for Cu, Ag and Au are also shown in the last 2 columns.

Element	a_0 (a.u.)		B		C_{11}		C_{12}		C_{44}		a (a.u.) $\approx 0.88a_0$	P_a
	Calc.	Exp.	Calc.	Exp.	Calc.	Exp.	Calc.	Exp.	Calc.	Exp.		
Cu	6.70	6.82	1.06	1.37	1.46	1.68	0.86	1.22	0.76	0.75	5.96	72.46
Ag	7.60	7.70	1.09	1.319	1.50	1.30	0.87	0.90	0.48	0.46	6.76	20.15
Au	7.67	7.71	1.81	1.69	1.95	1.89	1.74	1.59	0.40	0.42	6.83	81.31

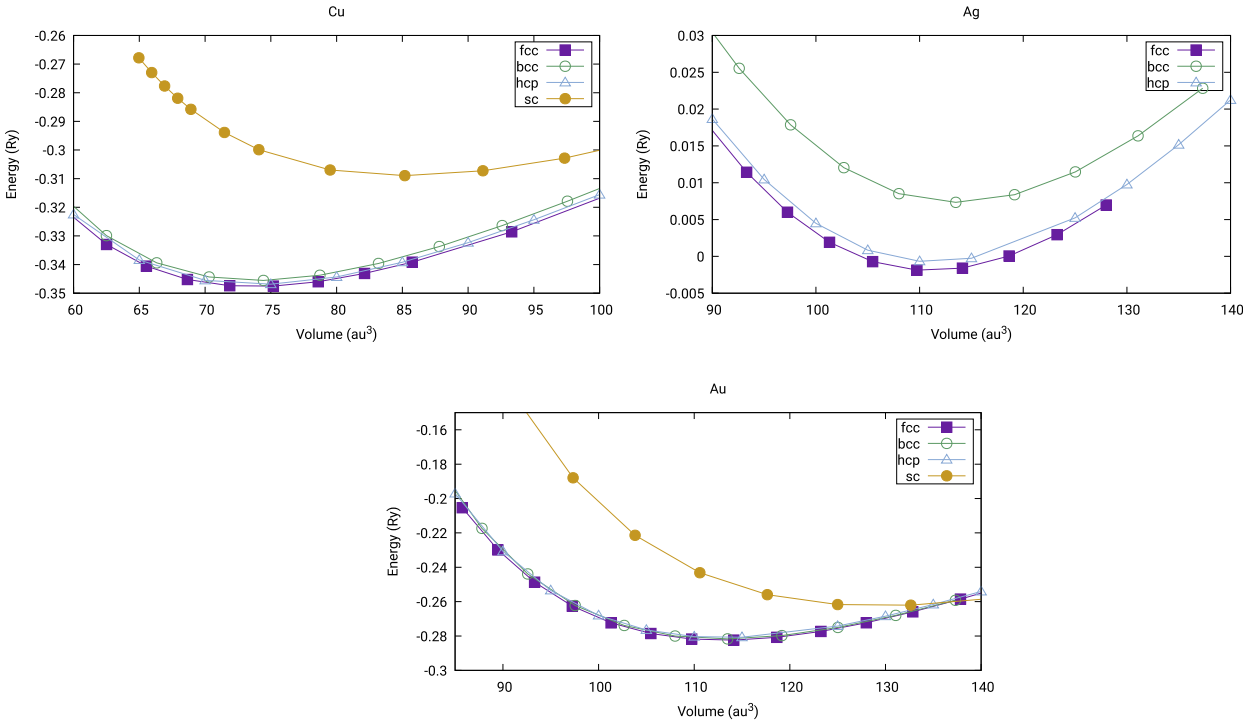

Fig. 2. The plots show the TB calculated energies over a range of lattice constant values for different crystal structures using the new parameters. The energy-volume dependence for Cu, Ag and Au follow the observed pattern [2] with the fcc being lowest. Energy values for the diamond structure (not shown) are higher up in the scale for all three.

in the three primitive lattice vectors to create the supercell. Starting at an initial kinetic temperature of $2T$, the atoms are assigned random velocities with a Boltzmann distribution function [4] and the simulation is run for a number of time steps. For each of the different temperatures, the atoms settle to velocities with greatly reduced fluctuations which correspond to approximately half the initial temperature; close enough to the target temperature T within an acceptable standard deviation [14]. A single time step was defined as $dt = 2$ fs. A typical calculation would run for about 2000 time steps with the first 500 steps excluded and the remaining steps used to calculate the time averages. For the cluster calculations, the positions of the nearest neighbors in an fcc structure from a reference atom extending from a low of 12 to 249 atoms were used and the system was relaxed using the conjugate gradient relaxation method mode of the TB-MD code. The energies are evaluated after the set tolerance was achieved or the set maximum number of iterations reached.

3. Results and discussion

3.1. DOS at finite temperature

To determine the DOS at each temperature, we collect the eigenvalues calculated at each time step of the MD run and bin them with a bin-width of 0.1 eV over all the k points included in the calculations. As we collect the eigenvalues, the position of the Fermi level at the various temperatures is also being calculated. In the resulting plots for Cu and Ag, shown in Fig. 3(a) and (c), the DOS is observed to change with increasing temperature. The changes, as shown in Fig. 3, are small, but more pronounced for the DOS at the Fermi level, E_f, as can be seen in the Fig. 3 (b) and (d).

3.2. Thermal expansion coefficient α

The theoretical value for the thermal coefficient α is determined by performing the MD simulations over a range of temperatures with the volume held constant. Assuming that the volume has a linear relationship with the varying temperature T, we use the calculated value for the bulk modulus B and so define the coefficient, α as

$$\alpha = \frac{1}{3B}\left(\frac{\partial P}{\partial T}\right)_V \tag{1}$$

The results, as seen in Table 2, show that we end up with values comparable with those measured [18] at room temperature for all three cases. The calculations are in perfect agreement with experiment for Au values whereas the Cu values are overestimated and the Ag underestimated.

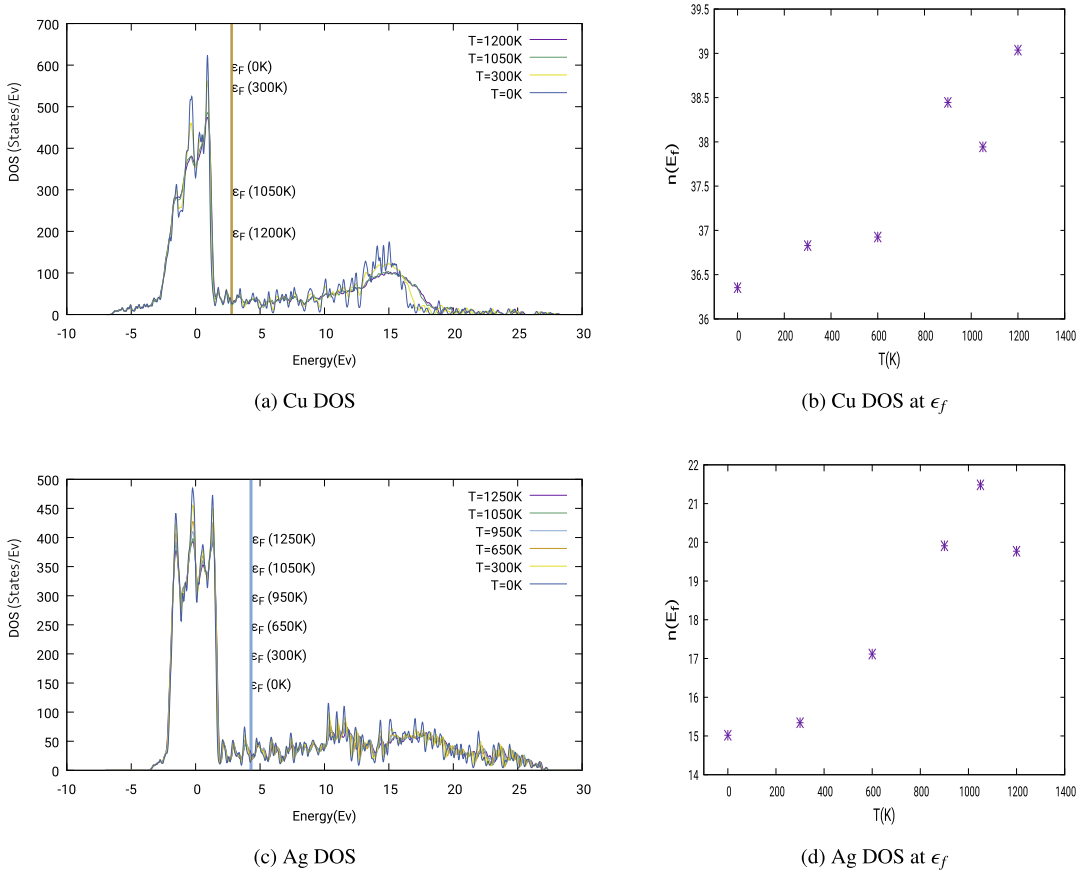

(a) Cu DOS

(b) Cu DOS at ϵ_f

(c) Ag DOS

(d) Ag DOS at ϵ_f

Fig. 3. Electronic density of states for Ag and Cu over a range of temperatures as generated from the eigenvalues calculated by the TBMD code. Each supercell held 125 atoms and the calculations were done for 4 *kpoints* in each case. For both cases, we can see the DOS increases with temperature at the Fermi level.

Table 2
Thermal expansion coefficient values calculated for the three noble metals Cu, Ag and Au in units of K^{-1} as compared to values measured at room temperature [18].

Element	Calc.	Exp.
Cu	2.50E−05	1.80E−05
Ag	1.07E−05	2.00E−05
Au	1.43E−05	1.40E−05

3.3. Debye-Waller factor

The TBMD calculations give us the mean square displacement $\langle u_x^2 \rangle$ of the atoms at different temperatures. From this we are able to calculate the Debye-Waller factor, $\boldsymbol{B}$, using the equation

$$\boldsymbol{B} = 8\pi^2 \langle u_x^2 \rangle = \frac{8\pi^2}{3} \langle |r^2| \rangle \tag{2}$$

Comparing the calculated results to experimental data in Fig. 4, we see that from lower through to higher temperature values close to room temperature, the calculated values track the experimental [19] quite well.

3.4. Vacancy formation energies

The TBMD code was also used to calculate the energies of vacancy formation for bulk cells as well as the energy for clusters. To determine the energy for single and double vacancies, with n being the number of vacancies, we used the relation (Eq. (3)):

$$E_{vac}(V) = E_{sc}(N-n, n; V) - (N-n)E_{bulk}(V/N) \tag{3}$$

Here $E_{sc}(N-n, n; V)$ is the total energy for a configuration of volume V with $N-n$ particles and n vacancies. E_{bulk} is the energy per atom of the bulk material. After creating the vacancy by removing n atoms, the TBMD simulation is run at constant temperature of $T = 0$ K to allow the supercell to relax as the atoms shift to compensate for the vacancy. By comparing the final energies with and without the vacancies, we determine the energy of vacancy formation E_{vac}.

From the calculated vacancy formation energies (shown in Table 3) we were able to observe the expected increase in the vacancy formation energy as the number of vacancies n was increased. The values were also close to those observed experimentally [20] with the E_{vac} for Ag overestimated in our calculations.

3.5. Phonon frequencies at finite temperature

The initial calculations to check the energy differences relative to the atomic displacement from the origin for the atoms in our supercell were done using the frozen phonon method at $T = 0$ K and a size of 4 atoms for the Δ, Σ and W points and 2 atoms for the Λ and X points. The phonon frequencies thus calculated were compared to experimental values and were found to agree quite well with the experimental results for Cu, Ag and for Au [21–23].

Next, using the TBMD code we calculated the phonon frequencies for a range of temperatures. This was done by initializing our supercell with lattice parameters and a number of ions depending on the temperature and symmetry direction of interest. The supercell grid was created by translating the lattice parameters by a factor of the lattice constant four times in each direction. After defining the ionic positions at the start of the simulation for each

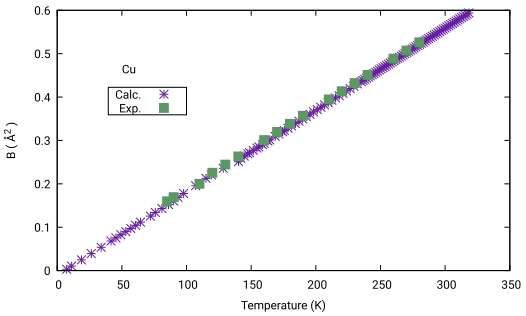

(a) Cu

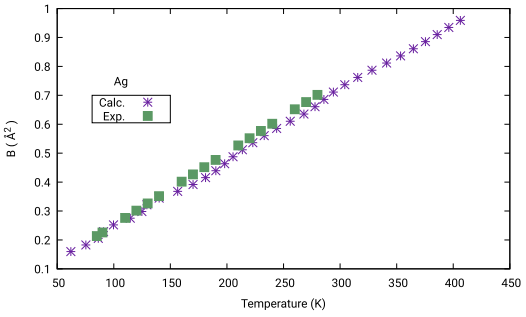

(b) Ag

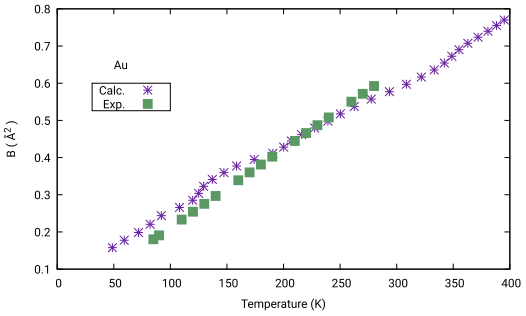

(c) Au

Fig. 4. The Debye-Waller factor for Cu, Ag and Au at different temperatures calculated from the TBMD simulation and how they compare to the experimentally observed data [19].

phonon frequency (4 for the Δ, Σ and W and 2 for the Λ and X), the ions were systematically displaced. The TBMD simulation was then run for a fixed number of time steps to calculate the total energies relative to displacement from the origin at the different temperatures.

Table 3
Vacancy formation energies for $n = 1, 2$ in eV for a supercell with 125 initial atoms for Cu, Ag and Au.

	E_{vac} for n vacancies		
	$n = 1$	$n = 2$	Expt. ($n = 1$) [20]
Cu	1.742	3.436	1.28
Ag	2.994	5.507	1.11
Au	1.314	2.525	0.89

To expand the lattice constant accordingly, we refer back to Table 2 for the calculated thermal expansion coefficients α_{Cu}, α_{Ag} and α_{Au} for the three different noble metals and using:

$$\alpha(a_{T_0}\Delta T) + a_{T_0} = a_T \tag{4}$$

where a_{T_0} is the lattice constant at $T = 0$ K and ΔT the temperature shift, we are able to determine the approximate value of the expanded lattice constant a_T at temperature T.

The TBMD calculations result in phonon frequencies that are, as shown in Table 4, in good agreement with the experimental results [21–23]. The values for $\Delta_1, \Delta_5, \Lambda_2, \Lambda_3, \Sigma_1, \Sigma_2, \Sigma_3$ were calculated at their mid-points. We are able to observe the general downward shift in the calculated values as the temperature is increased for all three noble metals.

3.6. Cluster energies

As with the other properties discussed in the previous sections, we emphasize that no cluster energies were fitted to DFT. Our results are a direct output of our TB Hamiltonian and they are in impressive agreement with the results of independent Quantum Espresso (QE) [24] calculations we performed.The QE code uses first principles pseudo potential methods within DFT.

To calculate and compare cluster binding energies, the simulation was run using the TB parameters and conjugate gradient method to relax initial configurations of different sized fcc-based, bcc-based and icosahedron clusters.

Fcc cluster configurations were generated based on the nearest neighbor positions from a reference atom in the fcc crystal structure to create clusters of size 13, 19, 43, 55, 79, 87, 135, 141, 177, 201, 225 and 249 atoms. To run the TB simulation, the lattice constant of the fcc primitive cell used for the relaxation is set as a large factor ($a = 8a_0$) of the previously calculated (shown in Table 1) equilibrium lattice constants, a_0, to ensure that the clusters are spaced far enough apart at the start. The resulting cluster energies after the conjugate gradient relaxation were observed to

Table 4
Calculated phonon frequencies in THz at different temperatures in K for Cu, Ag and Au. The values approximate the experimental values [21–23] accurately and the expected shift as the temperature changes is observed. The experimental values are taken at 80 K for Cu [21], 296 K for Ag [22] and 295 K for Au [23].

	Cu					Ag					Au				
	Exp.	0.000	300	600	900	Exp.	0.000	300	600	900	Exp.	0.000	300	600	900
Δ_1	6.2	5.851	5.524	5.215	5.015	4.93	4.999	5.157	5.125	5.109	3.4	3.366	3.537	3.518	3.235
Δ_5	4.2	3.616	3.41	3.432	4.165	3.76	3.813	4.117	3.997	3.969	1.5	1.829	1.923	1.986	1.761
Λ_2	7.4	8.814	8.781	8.409	8.081	7.9	8.026	8.405	8.352	8.326	4.6	5.487	5.805	5.771	5.311
Λ_3	3.4	3.463	4.002	3.922	4.138	3.68	3.726	4.013	3.91	3.879	1.8	1.961	2.328	2.305	2.212
Σ_1	6.5	7.261	6.572	6.592	6.282	6.51	6.614	7.052	6.848	6.644	3.9	4.254	4.304	3.891	3.478
Σ_2	3.5	3.646	3.682	3.379	3.523	3.69	3.739	3.97	3.864	3.812	1.4	1.781	1.871	1.803	1.742
Σ_3	5.2	4.738	4.902	4.746	4.401	4.99	5.078	5.673	5.515	5.435	2.1	2.884	2.977	2.963	2.68
W_2	4.9	5.144	5.317	5.277	5.238	5.22	5.302	5.935	5.774	5.682	2.6	2.629	3.067	3.049	2.756
W_5	6.2	6.405	6.236	6.189	6.144	6.42	6.527	7.276	7.068	6.965	3.6	4.036	4.345	4.316	3.935
X_3	7.3	8.633	7.874	7.815	7.758	7.81	7.935	8.677	8.434	8.327	4.6	5.425	5.712	5.678	5.262
X_5	5.1	5.221	4.802	4.766	4.732	5.25	5.324	5.446	5.321	5.248	2.6	2.889	2.964	2.944	2.693

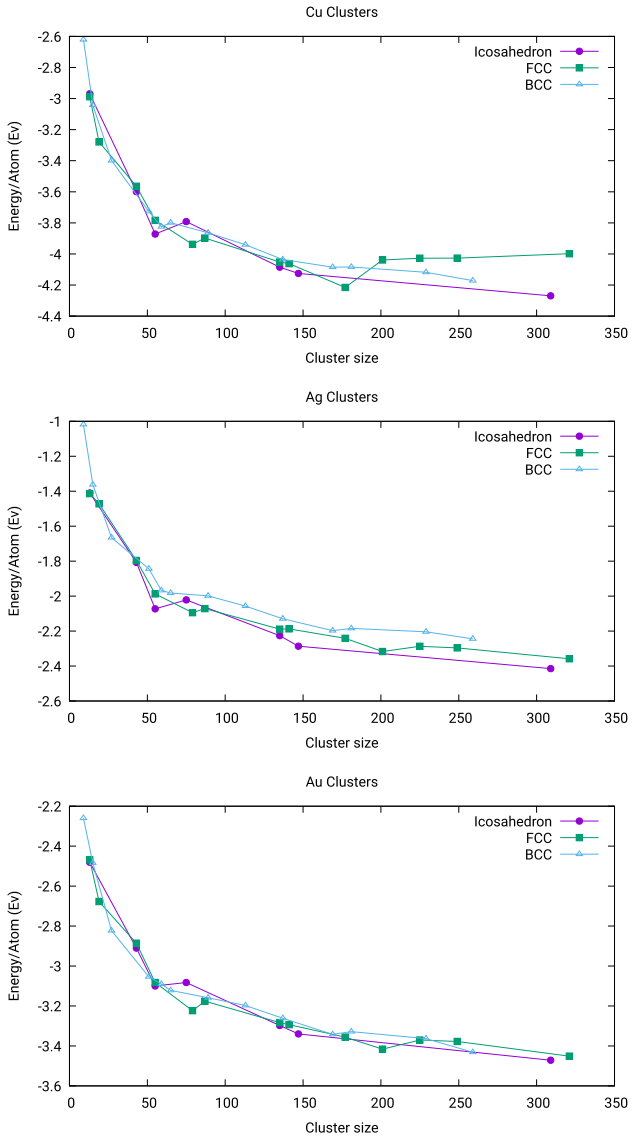

Fig. 5. The energy values calculated using the new TB parameters for different sized icosahedral, fcc-based and bcc-based clusters show the expected decrease with increase cluster size. As we increase the size of the cluster, the observed values should approach the bulk energies.

reduce as the cluster size was increased. The trends are shown in Fig. 5 for all three elements.

To generate the bcc cluster configurations, we used the nearest neighbor positions in the bcc crystal structure and created 9,15, 27, 51, 59, 65, 89, 113, 137, 169 and 181 atom sized bcc clusters. These configurations were used in the simulation, again setting the lattice constant of the bcc primitive cell at a similar factor as the fcc clusters.

The minimized energies for mackay-icosahedron clusters of sizes $n = 13, 43, 55, 75, 135, 147$ were also calculated for the three elements and compared to the fcc-based and bcc-based clusters. The same conjugate gradient relaxation was run for the different sized clusters, this time initialized in the icosahedral configurations. As can be seen from Fig. 5, the resulting energies for similar sized clusters for all the three cases fell within close range of each other.

We compared the calculated cluster binding energies to cluster binding energies calculated using the QE code. The same initial fcc-based,bcc-based and mackay-icosahedron cluster configurations of different sizes were used for both calculations. As shown in Fig. 6, the cluster energies calculated using the TB parameters compare quite well to those calculated using the independent first principles methods. For the cases of Ag and Au, they follow the same trend but with a shift so that the QE calculated energies are lower. The Cu energies are matched almost exactly with the QE results.

Taking the final configurations of the relaxed clusters from both the TB parameters and independent first principles QE calculations, we calculated the shell distances from the central atom for the different clusters and compared the two cases. From Fig. 7, we can see that the shell distances resulting from the TB parameters are in very good agreement with the QE results. This observation holds for the different sizes of clusters for all three elements. With the bcc-based clusters, both calculations show the same behavior at $n = 51$ where the first shell and second shells are switched. We have no explanation for this switch but it is interesting that this is happening in both the TB and QE calculations. For the mackay-icosahedron clusters, there is a slight shift in the calculated second shell distances for clusters of size $n > 43$ for the case of Au while the Ag and Cu show excellent agreement.

4. Conclusions

To summarize, a new set of TB parameters for the noble metals Cu, Ag and Au was obtained that enabled us to extend the simulation to even smaller inter-atomic distances. Utilizing these new parameters we performed TBMD simulations from which we calculated bulk moduli and elastic constants for the elements. We also calculated the DOS at finite temperature, mean squared displacements from which we determined the Debye-Waller factor and the thermal expansion coefficient. Comparing the calculated values to experimental data verified their accuracy as they were in agreement. Additionally, we calculated the energies for single and double vacancy formation that gave reasonable results when compared to both results calculated using TB methods as well as experimental observations.

We performed the TBMD simulation at finite temperature to calculate phonon frequencies using the previously calculated expansion coefficients to determine the corresponding expanded

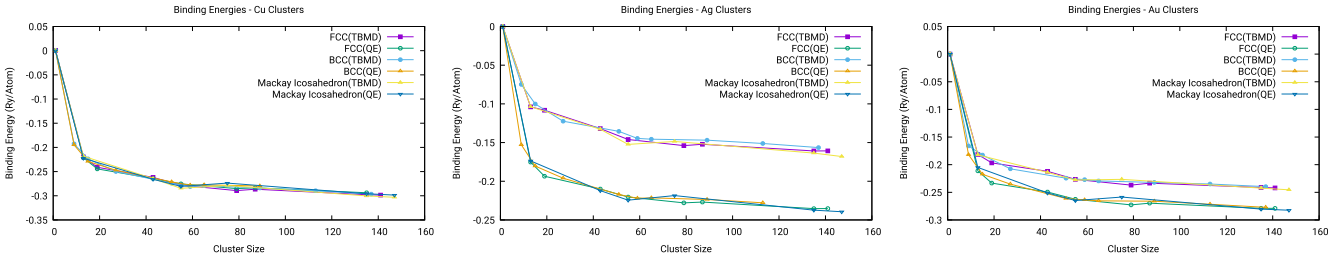

Fig. 6. Energies calculated for different fcc-based and bcc-based cluster sizes using the TB parameters compared to the same sized cluster binding energies calculated using QE. The TB parameters result in comparable energies to the QE first principles calculations, with Cu showing the best fit and Ag having the greatest shift.

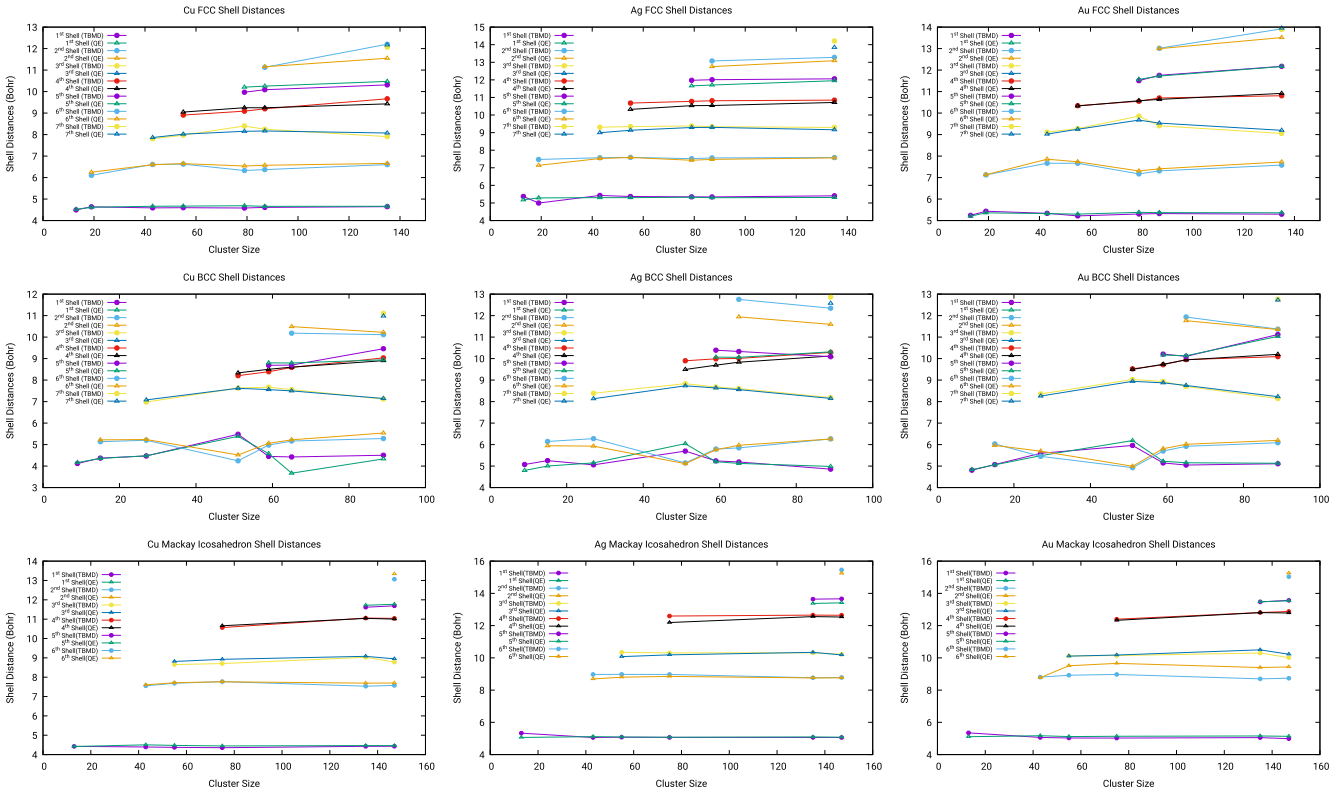

Fig. 7. Shell distances for the fcc-based, bcc-based and mackay-icosahedron clusters after relaxation using the TBMD parameters and the QE code showed excellent agreement. At cluster size $n = 51$ for the bcc-based clusters, the 1st and 2nd shells are switched in both calculations. The largest shift for the mackay-icosahedron occurs at the 2nd shell for Au.

lattice constants. The resulting phonon frequencies at different temperature values showed good agreement with experimental values and even had the expected downward shift as the temperature was increased.

The conjugate gradient relaxation method was also used to calculate icosahedral, fcc-based and bcc-based cluster energies which were seen to decrease as the cluster size is increased while approaching the bulk energies calculated for the supercell for all three noble metals. Comparing the icosahedral, fcc-based and bcc-based cluster energies to calculations done using the first principles methods based code QE resulted in similar trends, with Cu cluster energies showing excellent agreement with the DFT results and the Au and Ag being shifted upward. Calculated shell distances of the relaxed clusters also matched the results from independent first principles cluster calculations done using the QE code.

The results confirm that the new parameters are robust and produce results that are consistently accurate for the three elements investigated. As it is, we were able to demonstrate that with the new parametrization the TBMD model we apply is able to accurately predict dynamical properties of different materials at finite temperature.

Acknowledgements

D.P. acknowledges support by the U.S. Department of Energy grant DE-SC0014337.

M.M. is supported by the Kinnear Foundation and a contract from Duke University.

Appendix A. Equations and parameters

We present here the basic equations and parameters used in the non-orthogonal NRL-TB calculations.

The λ parameter is an atom type specific parameter in the description of a density ρ which describes the local environment around each atom [2]

$$\rho_i = \sum_{j \neq i} exp[-\lambda Rij] F_c(R_{ij})$$

where R_{ij} is the distance between atoms i and j, and F_c is the cutoff function.

The onsite term for each atom i is described as

$$h_l = a_l + b_l \rho_i^{\frac{2}{3}} + c_l \rho_i^{\frac{4}{3}} + d_l \rho_i^2$$

with l being the corresponding orbital.

The Hamiltonian and Overlap parameters listed in the Tables A.5, A.6 and A.7 are used in the expanded SK parameters function which includes the quadratic term as

$$P_{ll'u} = \left(e_{ll'u} + f_{ll'u} R + \bar{f}_{ll'u} R^2\right) \exp\left[-g^2_{ll'u} R\right] F_c(R)$$

where $ll'u$ is the type of interaction e.g. $ss\sigma$, and F_c and R are as described above.

Table A.5
Cu parameters.

λ	1.46E+00			
Onsite parameters				
l	a_l	b_l	c_l	d_l
s	2.91E−02	6.09E+01	−5.81E+03	2.26E+05
p	3.45E−01	8.88E+01	−6.28E+03	1.76E+05
t_{2g}	−2.91E−03	−2.80E+00	4.40E+02	−1.33E+04
eg	−2.91E−03	−2.80E+00	4.40E+02	−1.33E+04

Hamiltonian parameters					Overlap parameters				
$H_{ll'u}$	$e_{ll'u}$	$f_{ll'u}$	$\bar{f}_{ll'u}$	$g_{ll'u}$	$O_{ll'u}$	$e_{ll'u}$	$f_{ll'u}$	$\bar{f}_{ll'u}$	$g_{ll'u}$
$H_{ss\sigma}$	−5.97E+00	1.57E+00	−4.47E−01	9.68E−01	$O_{ss\sigma}$	−1.88E+00	1.00E+00	2.95E−01	9.63E−01
$H_{sp\sigma}$	1.42E+00	1.11E−01	2.09E−02	8.16E−01	$O_{sp\sigma}$	3.50E+01	−1.30E+01	6.07E−01	9.87E−01
$H_{pp\sigma}$	−7.00E−01	6.86E−01	−2.84E−02	7.66E−01	$O_{pp\sigma}$	4.70E+01	−1.50E+01	4.24E−01	1.03E+00
$H_{pp\pi}$	−1.95E−02	−1.58E+00	3.01E−01	9.43E−01	$O_{pp\pi}$	−4.53E+01	2.13E+01	−2.22E+00	9.74E−01
$H_{sd\sigma}$	−4.87E−01	−1.23E−01	−2.83E−02	9.26E−01	$O_{sd\sigma}$	1.86E+00	−1.02E+00	3.62E−02	1.14E+00
$H_{pd\sigma}$	−2.90E−01	−7.16E−02	1.38E−03	7.43E−01	$O_{pd\sigma}$	1.51E+00	−6.49E−01	−3.02E−01	1.08E+00
$H_{pd\pi}$	−1.87E+00	8.28E−01	1.29E−01	1.05E+00	$O_{pd\pi}$	−8.25E+00	7.37E−01	2.03E−02	1.02E+00
$H_{dd\sigma}$	−2.64E+00	6.13E−01	−4.11E−02	8.11E−01	$O_{dd\sigma}$	5.53E+00	8.60E−02	−3.04E−01	1.02E+00
$H_{dd\pi}$	6.97E+00	−1.74E+00	1.68E−01	1.01E+00	$O_{dd\pi}$	−8.56E+00	4.14E−01	5.61E−01	1.20E+00
$H_{dd\delta}$	−1.22E−01	−1.07E−01	−5.74E−02	1.14E+00	$O_{dd\delta}$	8.37E−02	−3.08E−01	7.54E−02	9.84E−01

Table A.6
Ag parameters.

λ	1.21E+00			
Onsite parameters				
l	a_l	b_l	c_l	d_l
s	1.78E−01	9.95E+00	3.37E+01	−2.70E+02
p	6.51E−01	1.47E+01	5.99E+01	−2.47E+03
t_{2g}	3.19E−03	1.06E−01	−2.24E−01	−9.36E+01
e	3.19E−03	1.06E−01	−2.24E−01	−9.36E+01

Hamiltonian parameters					Overlap parameters				
$H_{ll'u}$	$e_{ll'u}$	$f_{ll'u}$	$\bar{f}_{ll'u}$	$g_{ll'u}$	$O_{ll'u}$	$e_{ll'u}$	$f_{ll'u}$	$\bar{f}_{ll'u}$	$g_{ll'u}$
$H_{ss\sigma}$	−2.70E+00	2.98E−01	−1.20E−02	7.75E−01	$O_{ss\sigma}$	5.40E+00	−2.68E−01	−5.51E−02	8.41E−01
$H_{sp\sigma}$	2.66E+00	−3.56E−02	2.78E−03	7.84E−01	$O_{sp\sigma}$	−1.41E+00	−5.81E−02	4.90E−02	7.88E−01
$H_{pp\sigma}$	−1.43E+01	4.76E+00	4.99E−02	8.81E−01	$O_{pp\sigma}$	−7.61E−01	−1.31E−01	−4.96E−02	9.63E−01
$H_{pp\pi}$	8.00E+03	4.40E+02	−5.68E+01	1.53E+00	$O_{pp\pi}$	−6.19E+02	1.28E+03	−5.45E+01	1.48E+00
$H_{sd\sigma}$	−9.71E−01	9.02E−02	−1.54E−03	7.15E−01	$O_{sd\sigma}$	−1.28E+01	−4.90E+00	−1.18E+00	1.20E+00
$H_{pd\sigma}$	4.09E+00	−1.46E+00	−7.23E−04	8.95E−01	$O_{pd\sigma}$	−1.46E+01	1.61E+00	−8.07E−02	8.94E−01
$H_{pd\pi}$	7.28E−02	1.52E−01	6.15E−02	1.00E+00	$O_{pd\pi}$	−1.89E+00	2.61E−01	−5.21E−04	6.99E−01
$H_{dd\sigma}$	−7.41E−01	−1.10E+00	9.07E−03	9.82E−01	$O_{dd\sigma}$	1.44E+01	−2.50E+00	−7.91E−03	8.62E−01
$H_{dd\pi}$	8.81E+00	−8.11E−01	4.95E−02	1.03E+00	$O_{dd\pi}$	−1.04E+01	2.49E−01	7.28E−02	1.04E+00
$H_{dd\delta}$	1.71E+02	−2.24E+01	−3.39E+00	1.35E+00	$O_{dd\delta}$	6.09E+01	−8.30E+00	−4.55E−01	1.07E+00

Table A.7
Au parameters.

λ	1.39E+00			
Onsite parameters				
l	a_l	b_l	c_l	d_l
s	7.50E−02	1.62E+01	−4.11E+02	4.68E+04
p	4.57E−01	7.45E+01	−1.39E+03	2.63E+04
t_{2g}	−7.50E−03	−2.37E−01	1.20E+02	−3.08E+03
e_g	−7.50E−03	−2.37E−01	1.20E+02	−3.08E+03

Hamiltonian parameters					Overlap parameters				
$H_{ll'u}$	$e_{ll'u}$	$f_{ll'u}$	$\bar{f}_{ll'u}$	$g_{ll'u}$	$O_{ll'u}$	$e_{ll'u}$	$f_{ll'u}$	$\bar{f}_{ll'u}$	$g_{ll'u}$
$H_{ss\sigma}$	−1.10E+00	−4.93E−01	−1.25E−01	9.06E−01	$O_{ss\sigma}$	−5.21E+00	6.95E−01	5.17E−01	9.46E−01
$H_{sp\sigma}$	1.97E+00	−1.48E−01	−5.26E−03	6.99E−01	$O_{sp\sigma}$	1.12E+01	−1.89E+00	−4.90E−01	1.07E+00
$H_{pp\sigma}$	−3.04E+00	1.56E+00	1.48E−01	8.97E−01	$O_{pp\sigma}$	3.61E+02	3.38E+00	−2.95E+01	1.32E+00
$H_{pp\pi}$	1.69E+00	−1.89E+00	3.06E−01	8.46E−01	$O_{pp\pi}$	−7.88E+00	1.90E+00	2.99E−01	1.09E+00
$H_{sd\sigma}$	−1.17E+00	1.14E−01	−5.97E−04	6.79E−01	$O_{sd\sigma}$	9.22E+00	−3.33E+00	3.15E−01	8.16E−01
$H_{pd\sigma}$	1.78E+00	−1.39E+00	−1.84E−02	9.25E−01	$O_{pd\sigma}$	−1.96E+01	9.59E−01	9.27E−01	9.91E−01
$H_{pd\pi}$	4.00E+00	−8.36E−01	1.32E−01	9.97E−01	$O_{pd\pi}$	−3.81E+00	−2.44E−01	8.07E−02	1.06E+00
$H_{dd\sigma}$	−4.49E+00	4.06E−03	1.17E−02	8.99E−01	$O_{dd\sigma}$	7.36E−01	3.71E−01	6.92E−02	9.90E−01
$H_{dd\pi}$	7.85E+00	−5.14E−01	−2.80E−02	9.58E−01	$O_{dd\pi}$	−4.08E+00	−6.11E−01	1.55E−02	1.01E+00
$H_{dd\delta}$	−1.38E+01	4.09E+00	−3.75E−01	1.10E+00	$O_{dd\delta}$	3.69E+01	1.19E−01	−1.18E+00	1.21E+00

References

[1] J.C. Slater, G.F. Koster, Simplified LCAO method for the periodic potential problem, Phys. Rev. 94 (6) (1954) 1498–1524, https://doi.org/10.1103/PhysRev.94.1498.

[2] M.J. Mehl, D.A. Papaconstantopoulos, Applications of a tight-binding total-energy method for transition and noble metals: elastic constants, vacancies, and surfaces of monatomic metals, Phys. Rev. B 54 (7) (1996) 4519, https://doi.org/10.1103/PhysRevB.54.4519.

[3] R.E. Cohen, M.J. Mehl, D.A. Papaconstantopoulos, Tight-binding total-energy method for transition and noble metals, Phys. Rev. B 50 (19) (1994) 14694–14697, https://doi.org/10.1103/PhysRevB.50.14694.

[4] A. Shabaev, D.A. Papaconstantopoulos, Tight-binding molecular dynamics study of palladium, Phys. Rev. B – Condens. Matter Mater. Phys. 79 (6) (2009) 064107, https://doi.org/10.1103/PhysRevB.79.064107.

[5] D.A. Papaconstantopoulos, Handbook of the Band Structure of Elemental Solids, second ed., Springer, US, 2015, https://doi.org/10.1007/978-1-4419-8264-3.

[6] The NRL-Tight-Binding Codes. URL <http://esd.spacs.gmu.edu/tb/>.

[7] M. Kabir, A. Mookerjee, A.K. Bhattacharya, Structure and stability of copper clusters: a tight-binding molecular dynamics study, Phys. Rev. A 69 (2004) 043203, https://doi.org/10.1103/PhysRevA.69.043203.

[8] M. Menon, R.E. Allen, Simulations of atomic processes at semiconductor surfaces: general method and chemisorption on GaAs(1 1 0), Phys. Rev. B 38 (9) (1988) 6196–6205, https://doi.org/10.1103/PhysRevB.38.6196.

[9] J. Zhao, Y. Luo, G. Wang, Tight-binding study of structural and electronic properties of silver clusters, Eur. Phys. J. D 14 (2001) 309–316.

[10] A. Januszko, S.K. Bose, Phonon spectra and temperature variation of bulk properties of Cu, Ag, Au and Pt using Sutton-Chen and modified Sutton-Chen potentials, J. Phys. Chem. Solids 82 (2015) 67–75, https://doi.org/10.1016/j.jpcs.2015.03.008.

[11] A.P. Sutton, J. Chen, Long-range Finnis–Sinclair potentials, Philos. Mag. Lett. 61 (3) (1990) 139–146, https://doi.org/10.1080/09500839008206493.

[12] Y. Kimura, Y. Qi, T. Çagin, W.A. Goddard III, The Quantum Sutton-Chen Many-Body Potential for Properties of fcc Metals. URL <https://pdfs.semanticscholar.org/7b8f/de83e2716b6b0718cdcc581946eb4b39afc7.pdf>.

[13] G. Simmons, H. Wang, Single Crystal Elastic Constants and Calculated Aggregate Properties: A Handbook, second ed., MIT Press, Cambridge MA, 1971.

[14] F. Kirchhoff, M.J. Mehl, N.I. Papanicolaou, D.A. Papaconstantopoulos, F.S. Khan, Dynamical properties of Au from tight-binding molecular-dynamics simulations, Phys. Rev. B 63 (2001) 19501, https://doi.org/10.1103/PhysRevB.63.195101.

[15] S.H. Wei, H. Krakauer, Local-density-functional calculation of the pressure-induced metallization of BaSe and BaTe, Phys. Rev. Lett. https://doi.org/10.1103/PhysRevLett.55.1200.

[16] D. Singh, Ground-state properties of lanthanum: treatment of extended-core states, Phys. Rev. B. https://doi.org/10.1103/PhysRevB.43.6388.

[17] D.J. Singh, L. Nordstrom, Planewaves, Pseudopotentials and The LAPW Method, second ed., 2006. https://doi.org/10.1007/978-0-387-29684-5.

[18] Y. Touloukian, A Physicists Desk Reference – The Second Edition of Physics Vade Mecum, AIP, New York, 1989.

[19] L.-M. Peng, G. Ren, S.L. Dudarev, M.J. Whelan, Debye-Waller factors and absorptive scattering factors of elemental crystals, Acta Crystallogr. Sect. A 52 (1996) 456–470, https://doi.org/10.1107/S010876739600089X.

[20] D.A. Papaconstantopoulos, M.J. Mehl, The Slater–Koster tight-binding method: a computationally efficient and accurate approach, J. Phys.: Condens. Matter 15 (10) (2003) R413–R440, URL: stacks.iop.org/JPhysCM/15/R41.

[21] G. Nilsson, S. Rolandson, Lattice dynamics of copper at 80 K, Phys. Rev. B 7 (1973) 2393, https://doi.org/10.1103/PhysRevB.7.2393.

[22] W.A. Kamitakahara, B.N. Brcckhouse, Crystal dynamics of silver, Phys. Lett. A 29 (10) (1969) 639–640, https://doi.org/10.1016/0375-9601(69)91142-6.

[23] J.W. Lynn, H.G. Smith, R.M. Nicklow, Lattice dynamics of gold, Phys. Rev. B 8 (8) (1973) 3493–3499, https://doi.org/10.1103/PhysRevB.8.3493.

[24] P. Giannozzi, S. Baroni, N. Bonini, M. Calandra, R. Car, C. Cavazzoni, D. Ceresoli, G.L. Chiarotti, M. Cococcioni, I. Dabo, A. Dal Corso, S. De Gironcoli, S. Fabris, G. Fratesi, R. Gebauer, U. Gerstmann, C. Gougoussis, A. Kokalj, M. Lazzeri, L. Martin-Samos, N. Marzari, F. Mauri, R. Mazzarello, S. Paolini, A. Pasquarello, L. Paulatto, C. Sbraccia, S. Scandolo, G. Sclauzero, A.P. Seitsonen, A. Smogunov, P. Umari, R.M. Wentzcovitch, QUANTUM ESPRESSO: a modular and open-source software project for quantum simulations of materials, J. Phys. Condens. Matter. https://doi.org/10.1088/0953-8984/21/39/395502.